DOI: 10.13009/EUCASS2019-240

The Influence of Meteorological Conditions on the Icing Performance Penalties on a UAV Airfoil

Nicolas Fajt, Richard Hann* and Thorsten Lutz***
**Norwegian University of Science and Technology, 7034 Trondheim, Norway*
nicolsf@stud.ntnu.no · richard.hann@ntnu.no
***Universität Stuttgart, 70174 Stuttgart, Germany*
thorsten.lutz@iag.uni-stuttgart.de

Abstract
This paper presents a large parameter study on meteorological conditions to investigate the aerodynamic performance degradation of UAVs for a wide range of icing conditions. The knowledge about weather influences is essential for the development of efficient icing protection. The numerical CFD simulations for ice accretion and performance evaluation were performed on the 2D airfoil RG-15, using FENSAP-ICE. The method is validated with literature and experimental data. The results show a significant deterioration of lift and drag for all selected icing conditions and a distinct dependency of temperature, liquid water content and ice mass on the aerodynamic performance.

1. Nomenclature

AoA / α	=	Angle of attack	ρ_w	=	Water density
β	=	Collection efficiency	Re	=	Reynolds number
c	=	Chord length	t_{icing}	=	Icing time
I	=	Performance index	T_{icing}	=	Icing temperature
IPS	=	Icing protection system	T_w	=	Surface temperature
LWC	=	Liquid water content	τ_w	=	Surface shear stress tensor
MVD	=	Median volume diameter	u_d	=	Droplet velocity
$\dot{m}_{ice}$	=	Mass of ice accretion	u_∞	=	Free stream velocity
p	=	Air static pressure	Q	=	Heat flux

2. Introduction

Recent development has shown that atmospheric icing is one of the main operational limitations of small and medium-size fixed-wing unmanned aerial vehicles (UAVs) with a wingspan of approximately 2 to 4 m in their growing field of applications [1]. Ice accretions on airfoils changes the aerodynamic performance (e.g. lift, drag, stability, stall behavior) [2] and thereby limits flight capabilities such as range and duration. To ensure safe operation of UAVs, without icing protection systems, a common approach is to ground the aircrafts when icing conditions are expected [3].

A main challenge of UAV icing is that the well understood icing process of manned civil and military aircrafts does not apply to most UAVs. Due to the typically lower airspeed and smaller sizes, UAVs operate at a lower Reynolds number regime of Re = 1–10 x 10^5, whereas manned aviation is characterized by a Reynolds number regime of Re = 1–10 x 10^6 [2]. This difference implies the necessity to gain better understanding of the icing process at low Reynolds numbers.

The work by Szilder and McIlwain [4] with their morphogenetic icing model has shown that the ice shapes are strongly dependent on the Reynolds number. One major finding is that higher Reynolds numbers lead to a reduction of rime and increase of glaze ice in a parametric space, defined by air temperature and liquid water content. Further, a comparison of an airfoil traveling the same distance through icing conditions at various Reynolds numbers revealed that higher Reynolds numbers lead to significantly smaller ice extends. This implies the importance to separate studies on the ice accretion process of small-sized fixed-wing UAVs from general aircraft icing. Other commonly utilized tools for the ice accretion simulation on UAV airfoils are the NASA code LEWICE [5] and FENSAP-ICE [6]. A

DOI: 10.13009/EUCASS2019-240

comparison between LEWICE and FENSAP-ICE for UAVs has been covered by Hann [7]. It showed that both codes predict a significant decrease of maximum lift, stall angle and increase of drag for all three investigated icing cases (rime, glaze and mixed ice). However, the comparison also revealed limitations of the panel-method used within LEWICE. Whereas the ice shapes of both codes were congruent for the rime ice case, they deviate significantly for the mixed and glaze ice case. This in consequence, led to similar performance results for the rime ice case but discrepancies for the mixed and glaze ice case.

The aim of this study is to investigate the influence of various meteorological conditions on the aerodynamic performance of the RG-15, a typical UAV airfoil, using FENSAP-ICE. The above mentioned earlier work on UAV icing has shown that ice accretion affects the aerodynamic performance negatively, but no study has been conducted that investigates the relation of meteorological conditions to the degradation of performance. For successful development of an effective and efficient icing protection systems (IPS) for UAVs it is crucial to identify worst case icing conditions. Additionally, the knowledge about the influence of different icing conditions on the airfoil's performance is essential for the adaption of flight controllers, to enable safe flight in varying weather conditions and thereby extending the UAV's operational capabilities.

3. Methods

3.1 Numerical Methods

Two different simulation models are set up to capture the ice accretion and the performance of the iced airfoil. The first model generates an iced geometry which is the input geometry for the second model. This will, subsequently, be used to determine the aerodynamic performance of the iced airfoil. All simulations are performed with ANSYS FENSAP-ICE (version 2019 R1). The software package consists of several linked modules to obtain the ice accretion process. Within this work, the three modules FENSAP, DROP3D and ICE3D are used.

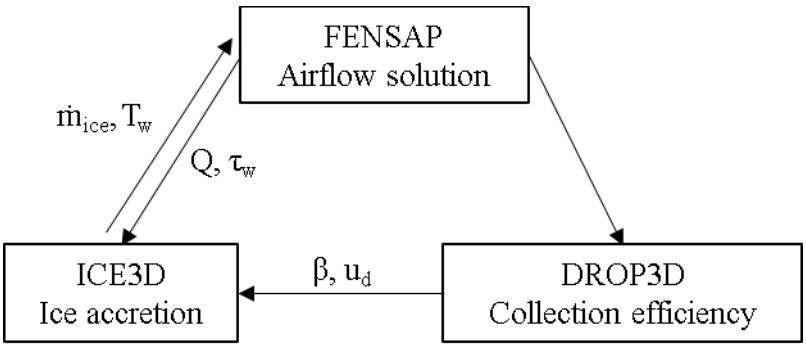

Figure 1: Linked modules of FENSAP-ICE from [10].

Figure 1 shows how the three modules interact with each other. **FENSAP** is a state-of-the-art CFD solver that obtains the airflow solution by solving compressible Reynolds Averaged Navier-Stokes (RANS), also called Favre-averaged equations [8]. The FENSAP CFD solver is used in both simulation models (to provide the flow solution). For the ice accretion FENSAP is utilized as part of the loop presented in Fig. 1, whereas for the simulation of aerodynamic performance, FENSAP is used as stand-alone system. Ultimately, all FENSAP simulations are set up with a streamline upwind artificial viscosity, to increase numerical stability. **DROP3D** is an Eulerian droplet impingement module. Based on the airflow solution, it solves partial differential equations to calculate the droplet velocity, collection efficiency and impingement limits [9]. **ICE3D** is solving partial differential equations, like the impingement module DROP3D [10]. ICE3D requires the shear-stresses and the heat flux distribution across the wing, obtained by FENSAP, as well as the mass of water, caught by DROP3D, to calculate the ice accretion. The ice shape acquired by the ICE3D module provides the new geometry, to be used by FENSAP for the next airflow calculation.

Following the efforts of Hann et al. [11] a Spalart Allmaras (SA) one-equation turbulence model with fixed transition is applied for the performance simulations of the clean/un-iced airfoil. This includes the clean airfoil simulation for the validation of the performance model. Additionally, a simulation with menter's two-equation k-ω-SST turbulence model, is set up for the validation.

Clean airfoil simulations using the SA model with fixed transition obtain the transition location from XFOIL [12]. In cases, where surface ice is present, an immediate transition from laminar to turbulent boundary layer is expected at the leading-edge, due to the increased surface roughness in comparison to an un-iced airfoil. Therefore,

DOI: 10.13009/EUCASS2019-240

simulations including ice, such as ice accretion and iced airfoil performance, are set up fully turbulent with the SA model.

Multishot ice accretion. The concept of FENSAP-ICE as interactive loop enables a segmentation of the overall icing duration into smaller time frames. This way, the influence of ice on the airflow, catch efficiency and further ice accretion is considered. ICE3D offers two different automatic remeshing processes to generate a displaced grid around the new ice shape: OptiGrid and Fluent remeshing. For this study Fluent remeshing was used, since it offers more control and stability on the remeshing process. OptiGrid is part of the FENSAP-ICE package and a fully automatic process that deforms the existing grid by moving nodes and coarsening and refining edges. Fluent remeshing on the other hand uses ANSYS FLUENT for a complete re-meshing of the new geometry after each step. Grid creation, grid control parameters and the interaction between FENSAP and FLUENT are covered by additional files in the simulation setup.

3.2 Grid setup

For the discretization of all airfoils in this study, Pointwise (version 18.2) has been used. The grids are set up as hybrid O-grid with a structured resolution of the boundary layer and an unstructured resolution of the farfield. The simulation of ice accretion requires a different grid setup than the simulation of aerodynamic performance. The different features of both types of grids are listed in Tab. 1 and shown in Fig. 2. Grid dependency studies have been conducted for both grid types to ensure independence of the results from the grids. Due to space restrictions, results of those studies are excluded from this paper.

Table 1: Grid features of ice accretion and performance grid.

Feature	Ice accretion grid	Performance grid
Grid dimension	3D	2D
Chord length *c*	0.45 m	0.45 m
Farfield diameter	9 m (20 c)	30 m (66.7 c)
Boundary layer resolution	Constant number of structured layers – 50 layers	Variable number of structured layers – ensures ideal isotropic cell height at the boundary from structured to unstructured grid
Spanwise discretization	Triangular elements – fine resolution of the leading-edge to capture the ice accretion	None – extrusion by one cell
Trailing edge resolution	Blunt – 1 mm height	Blunt – 1 mm height
Number of cells	~5 400 000	~80 000
Reference wing area	0.02025 m²	0.45 m²

Since the focus for the ice accretion grid is not on precise calculation of aerodynamic coefficients, a smaller farfield, a constant number of structured layers and a smaller spanwise extrusion is initialized, to keep the number of cells within reasonable range.

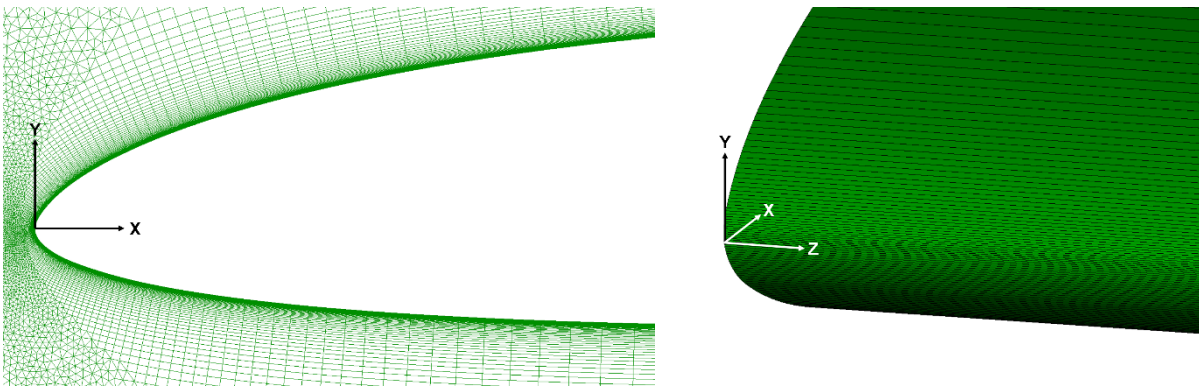

a)

DOI: 10.13009/EUCASS2019-240

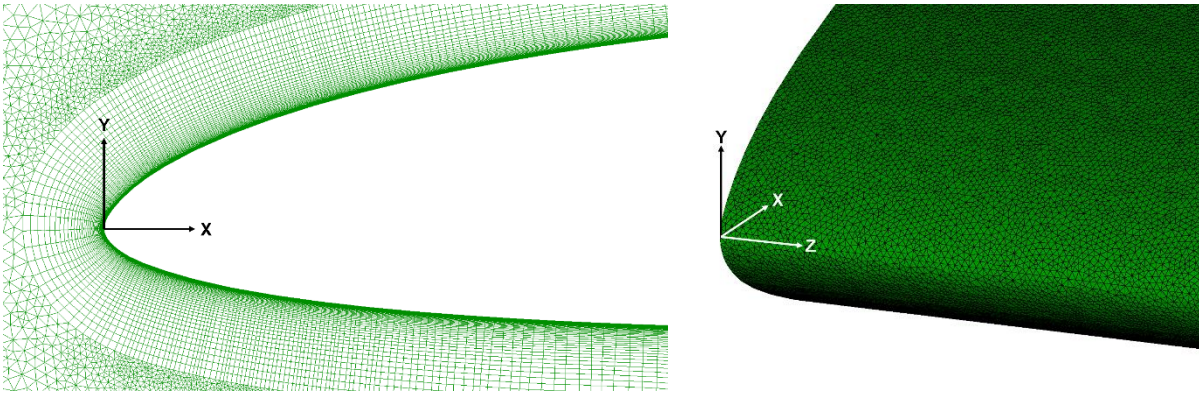

b)

Figure 2: Grid differences of a) performance and b) ice accretion grid.

3.3 Icing conditions

The CFR 14, Part 25, App. C [15], used for the certification of manned aircraft, offers two different envelopes that define the icing conditions for continuous maximum and intermittent maximum icing. The envelope for maximum continuous icing applies for cloud ceiling heights from 22000 ft (6700 m) down to sea level and therefore includes flight altitudes of small UAVs. For this reason, all icing cases investigated in this work are within the envelope of maximum continuous icing conditions of the Federal Aviation Administration (FAA) requirements. Figure 3 and Tab. 2 give an overview over the icing cases and the corresponding parameters.

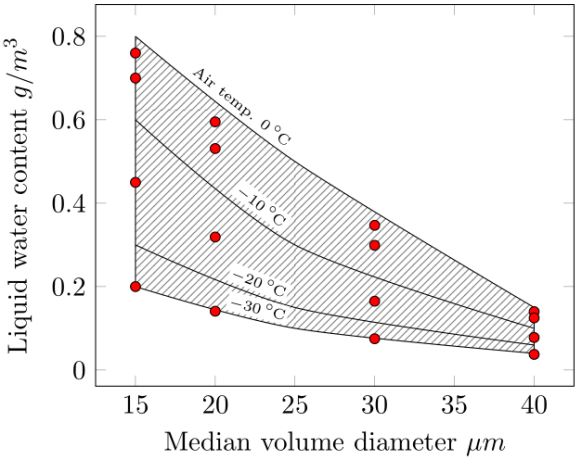

Figure 3: Icing case overview, modified from [15].

Table 2: LWC in g/m³ as function of MVD and temperature.

MVD [µm]	**T_{icing} [°C]**			
	-2	**-5**	**-15**	**-30**
15	0.760	0.700	0.450	0.200
20	0.595	0.531	0.319	0.141
30	0.347	0.299	0.165	0.070
40	0.140	0.125	0.078	0.038

The parameters cover a temperature range of -30 °C to -2 °C, a median volume diameter range of 15 µm to 40 µm and the corresponding liquid water content of 0.038 g/m³ to 0.760 g/m³. All ice accretion simulations are set up with a monodisperse droplet distribution. Constant values for the ice accretion simulations are summarized in Tab. 3. The icing time is determined by the cruising speed of 25 m/s and the maximum horizontal cloud extend of 17.4 nm.

Table 3: Constant parameters for the ice accretion simulations.

Parameter	**Value**
Free stream velocity u_∞	25 m/s
Icing time t_{icing}	1290 s
Angle of attack AoA	0°
Chord length c	0.45 m
Water density ρ_w	1000 kg/m³
Air static pressure p	95500 Pa ≙ 500 m flight altitude

DOI: 10.13009/EUCASS2019-240

4. Model validation

4.1 Clean / iced airfoil performance

The validation of clean airfoil performance is based on experimental data of two wind tunnel tests at a Reynolds number of Re = 200 000, published in [16] and [17]. Two simulations were performed using the k-ω-SST and the Spalart Allmaras (SA) turbulence model. For the k-ω-SST model transition is predicted by a one-equation local correlation-based intermittency model, whereas the SA turbulence model is set up with fixed transition locations, previously determined with XFOIL. The comparison of experimental and simulation results is presented in Fig. 4.

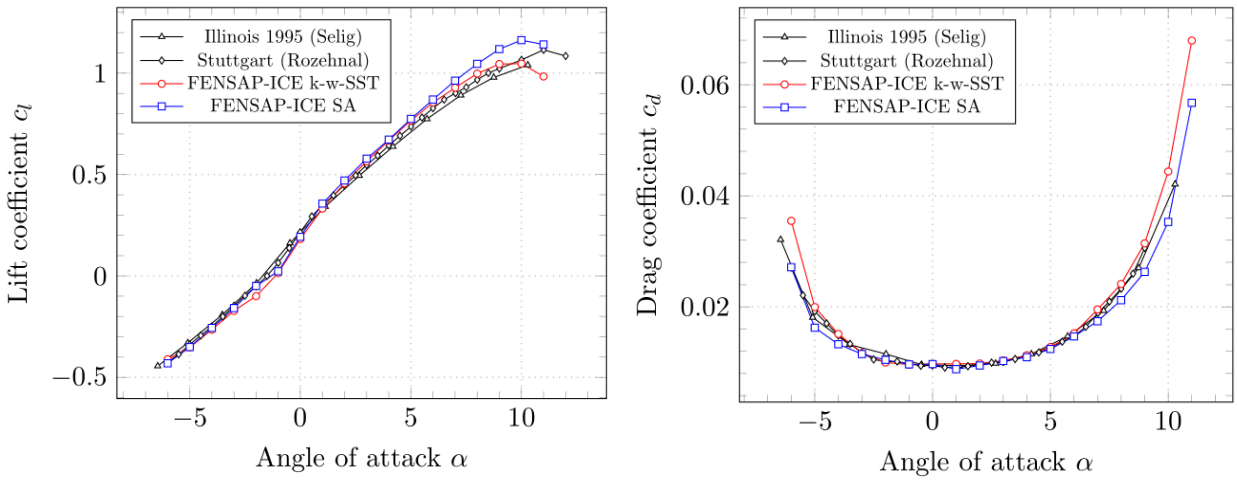

Figure 4: Validation of clean airfoil performance on a clean RG-15 airfoil – Re = 200 000.

Both simulation results show good general agreement with the experimental results. At AoAs from -3° to -1° both simulations show a minor deviation of predicted lift coefficients to the experimental data. A possible explanation could be that the simulations both predict slightly earlier transition from laminar to turbulent boundary layer.

The stall is captured within reasonable range to the experimental results with both turbulence models. The simulation model using the k-ω-SST model predicts a lower maximum lift coefficient and lower maximum lift angle, compared to the SA model. The tendency of estimating lower maximum lift coefficients and respective AoAs with the k-ω-SST model, has already been observed in previous work, by Hann et al. [11]. The drag prediction of both simulations shows good agreement to the experimental results for the whole AoA range. For AoAs >7°, with the onset of a stall, the k-ω-SST predicts higher drag compared to the SA model.

Since no suitable literature data of an iced RG-15 airfoil was found, wind tunnel test results of an iced NREL S826 airfoil at a Reynolds number of Re = 400 000, published in [13], were used for the validation of the performance simulation of an iced airfoil. The data for the iced NREL S826 are gathered by 3D-printing the ice geometry and attaching it to the clean airfoil for the wind tunnel tests. The simulation results are presented in Fig. 5.

DOI: 10.13009/EUCASS2019-240

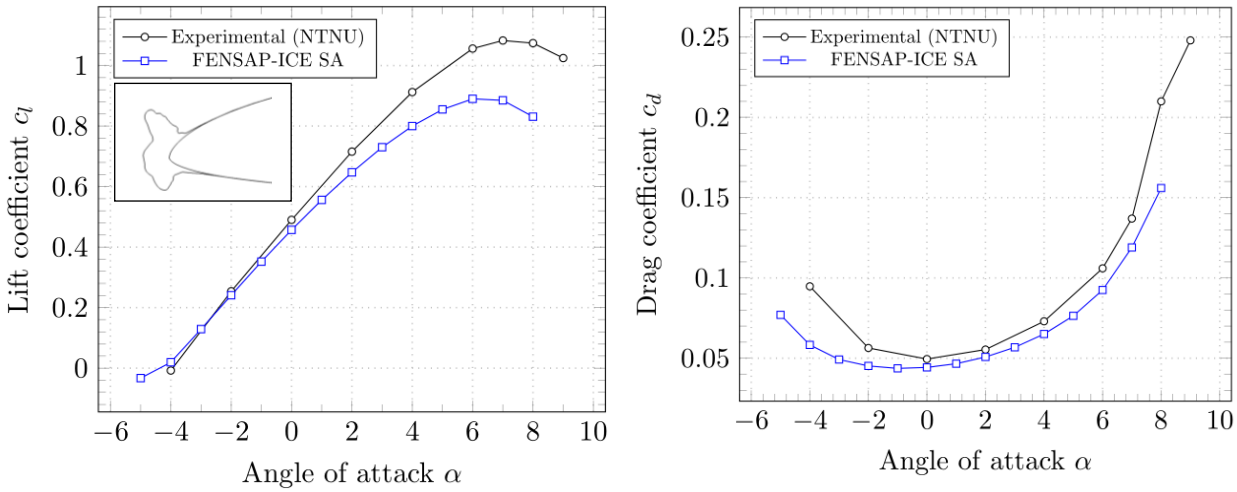

Figure 5: Validation of aerodynamic performance on an iced NREL S826 airfoil – Re = 400 000.

For the AoA range of -8° to 0° the simulation results for the lift show good agreement with the experimental data. Regarding the stall, the simulation predicts an earlier stall at a lower maximum lift coefficient and maximum lift angle. Further, the simulation shows a smaller lift gradient. Regarding the drag, the simulation captures a similar trend of drag over AoA but under-predicts the drag at all points. The reason for the diverting results is suspected to be in the use of the turbulence model (Spalart-Allmaras) in combination with a high level of turbulence, caused by the horns. The surface roughness and the horn shape results in a high level of turbulence and flow separation already at very low AoAs. For the degree of turbulence and separated flow from the leading-edge, like in this case, different numerical methods like LES and DNS or higher-level turbulence models like nonlinear eddy viscosity models and Reynolds stress models might be more suitable.

The icing conditions in this case have been specifically chosen to create severe icing with a horn shaped structure. To achive that, the several icing parameters were modified. In particular, the icing time was set to 40 minutes, twice of what is used in this work. For a detailed listing, see [13]. Therefore, a much smaller extend of ice and turbulence is expected for the icing cases in this work.

4.2 Ice accretion

For the validation of the ice accretion simulation, experimental data from an icing wind tunnel was available [14]. From those data two different conditions, presented in Tab. 4, were selected.

Table 4: Icing conditions for the validation of ice accretion.

Parameter	**Icing case**	
	Rime	Glaze
Free stream velocity u_∞	25 m/s	25 m/s
Chord length c	0.45 m	0.45 m
Icing time t_{icing}	1200 s	1200 s
Angle of attack AoA	0°	0°
Icing temperature T_{icing}	-15 °C	-2 °C
Median volume diameter MVD	20 µm	30 µm
Liquid water content LWC	0.51 g/m³	0.51 g/m³

These conditions represent a rime and a glaze ice case with their typical shapes. Rime ice has a more streamline shape and icing limits further upstream compared to glaze ice, due to instant freezing of all impinging water. Since a 3D airfoil was tested, for reasons of clarity, only one cross-section of the experimental result is shown in Fig. 6.

DOI: 10.13009/EUCASS2019-240

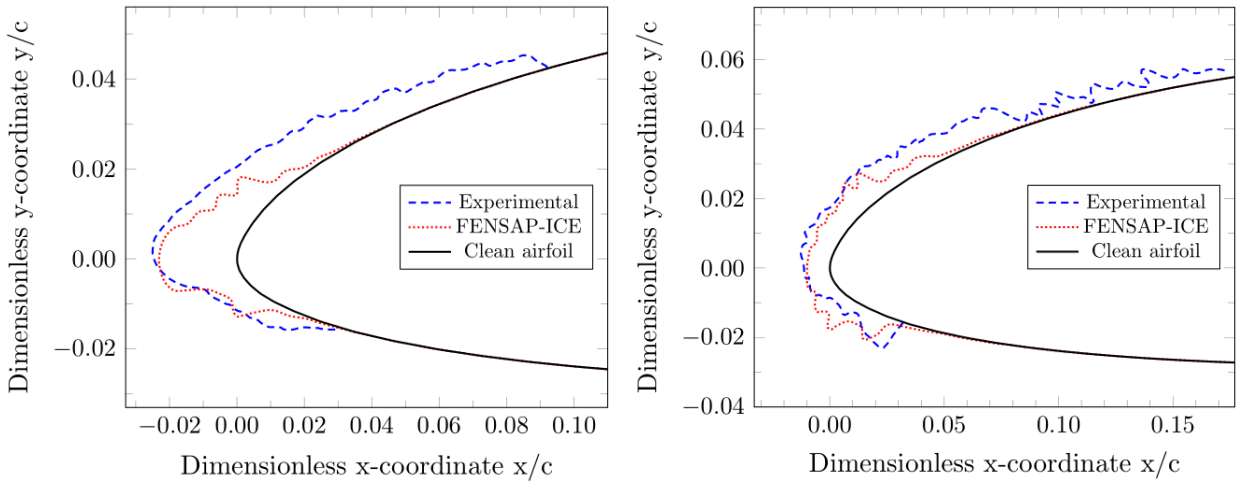

a) Rime ice **b) Glaze ice**

Figure 6: Ice shape results vs. experimental results for the a) rime ice and b) glaze ice case – Re = 800 000.

The simulation captures the lower icing limit and the expansion of ice accretion in x-direction correctly in both cases. However, the simulation predicts less ice and a further upstream icing limits compared to the experimental results. This supports the findings of Hann [7] that FENSAP-ICE under-predicts the upper icing limits. Further findings, that the simulation predicts a more regular and smooth ice shape could not be confirmed. The general ice shapes of the simulation results within this work, match the experimental results [14]. The under-prediction of upper icing limits could be caused by the wide variation of ice shapes for the experimental results. Besides the variation of experimental results on the RG-15 airfoil, Szilder and Yuan have already encountered a wide variation of ice shapes during experiments in the icing wind tunnel on a NACA0012 airfoil [18]. The SAE international group has also identified large variations of ice shapes, using the same weather conditions in different icing wind tunnel facilities [19].

Considering the generally good agreement and the wide variation of experimental results, the prediction of ice shapes is within reasonable range of the experimental results.

5. Results

5.1 Ice accretion

Figure 7 shows the ice shape results for all icing cases, specified in Tab. 2 and 3. For reasons of readability, the MVD will be mentioned without unit at some points.

The results show that both, liquid water content and droplet diameter have significant influence on the ice shape. As previously shown in Fig. 3, droplets with small MVDs around 15 µm can contain a higher range of liquid water content, compared to large MVDs. Therefore, the results at a temperature of -2 °C and droplet diameters 15, 20 and 30 show a distinct glaze ice shape with a rough surface. At a droplet diameter of 40 µm, the maximum liquid water content has decreased to a point, where all results show a streamline shaped ice geometry, independently from the prevailing temperatures. All results at the diameter of 40 µm are close to the un-iced airfoil geometry. The extend only differs slightly, in accordance with the present liquid water content at the different temperatures.

MVD 15, 20 and 30 share the same behavior with decreasing extend of the ice shape for decreasing temperatures from -5 °C to -30 °C. The change from -2 °C to -5 °C however, shows a different result for these three MVDs. The extend in x-direction is significantly increasing, while the extend in y-direction shrinks. Regarding the general geometry, this behavior marks the transition from a glaze ice to a more streamlined rime ice structure.

DOI: 10.13009/EUCASS2019-240

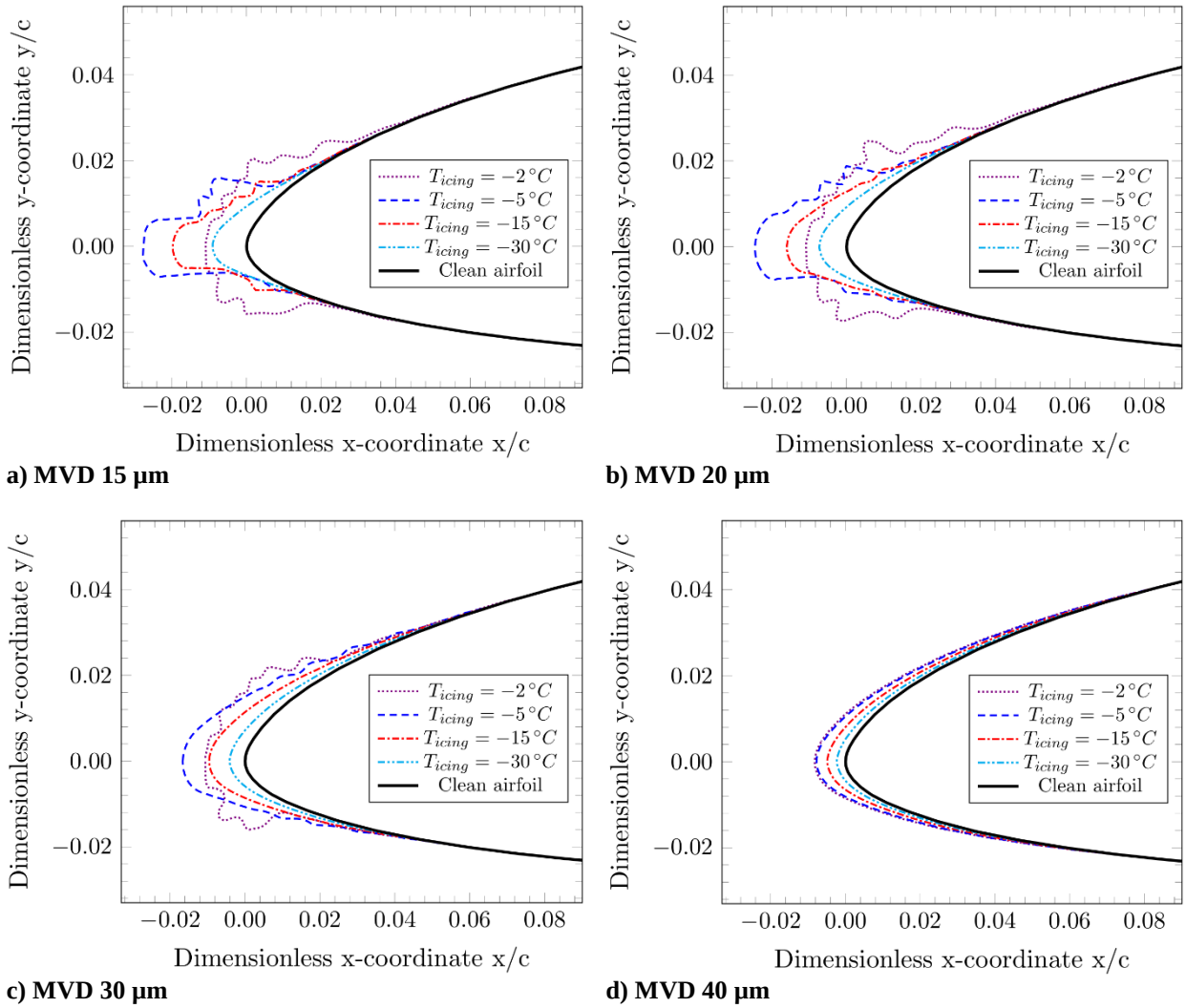

Figure 7: Ice shape results for droplet sizes a) 15 µm, b) 20 µm, c) 30 µm and d) 40 µm – Re = 800 000.

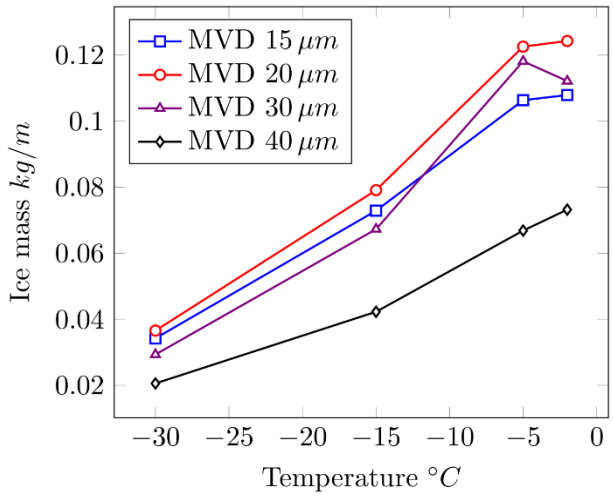

Figure 8: Accumulated ice mass from the simulation.

In terms of accumulated ice, Fig. 8 shows that the highest ice masses occur at an MVD of 20 µm and the lowest at an MVD of 40 µm. Since all simulations are 2D airfoil simulations, the resulting ice masses are considered as mass per wingspan extend. The results show a differentiated influence of droplet MVD and liquid water content on the

DOI: 10.13009/EUCASS2019-240

overall ice mass. Increasing the droplet size from 15 to 20 results in a higher ice mass, whereas the increase from MVD 20 to 40 results in lower ice mass, although the liquid water content decreases consistently. Comparing MVD 15 with 30, the results of MVD 30 µm show higher ice masses for temperatures -2 °C and -5 °C and lower ice masses for the temperatures -15 °C and -30 °C. This indicates that the shift from increasing droplet size to decreasing liquid water content being the dominating factor on the ice mass occurs at different droplet sizes, depending on the temperature.

All ice shapes, with one exception, show a shift of icing limits towards the leading-edge with decreasing temperatures. While all impinging water freezes instantly at low temperatures, the impinging water at temperatures close to 0 °C only freezes partially, leaving a liquid water film that runs downstream on the surface before freezing completely. This extends the icing limits to positions further away from the leading-edge. Solely the icing limit on the lower surface of the airfoil at an MVD of 30 µm and a temperature change from -2 °C to -5 °C shows a shift of the limit toward the trailing-edge. Finally, in all cases, except for one, larger droplets lead to further downstream icing limits.

5.2 Performance degradation

Based on the acquired ice shapes that were presented in the previous section, FENSAP simulations have been run to determine the performance of the iced airfoils. Figure 9 and 10 present the lift and drag coefficient of the iced airfoils in comparison to the clean airfoil. In general, the simulation predicts decreased lift and increased drag for all icing cases and the entire range of AoAs. The curves show a strong correlation between the aerodynamic performance and the iced airfoil's shape. For streamline shaped ice (e.g. ice shapes at an MVD of 40 µm), the simulation predicts smaller decrease of lift and increase of drag, compared to icing cases with rough surfaces and a larger ice shape extension in y-direction (e.g. MVD 15 µm and -2 °C icing temperature). Additionally, rime ice cases with more streamline shaped ice seem to have less effect on the maximum lift angle.

The maximum deterioration of lift, corresponding AoA and increase of drag occurs at -2 °C/MVD 20. In this icing case the lift coefficient decreases by 35 % and the AoA by 33 %, compared to the clean airfoil. Drag increases by 160 %. At the AoAs of 0° and 6° the lift coefficient decreases by 6.5 % and 12.5 % and the drag increases by 80.0 % and 90.5 % respectively.

The airfoil moment curves in Fig. 11 show increased moment gradients for all icing cases. As for lift and drag, higher temperatures in combination with high LWC values show greater influence on the moment, compared to lower temperatures and low LWC values.

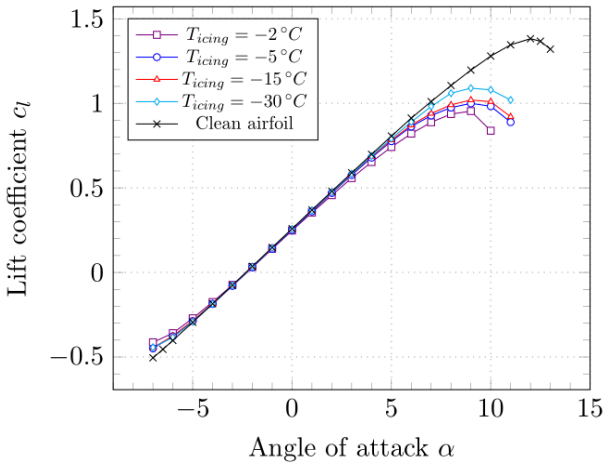

a) MVD 15 µm

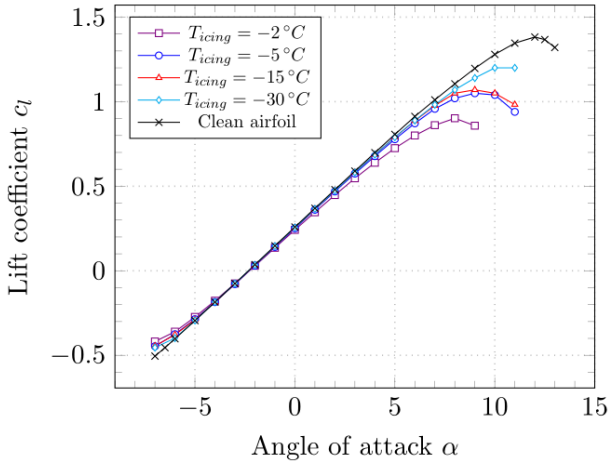

b) MVD 20 µm

DOI: 10.13009/EUCASS2019-240

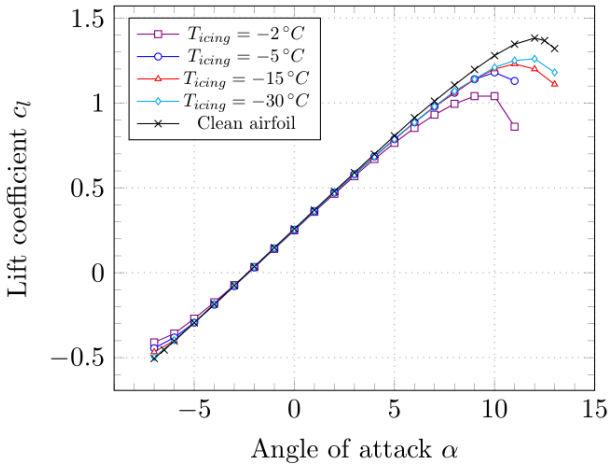

c) MVD 30 µm

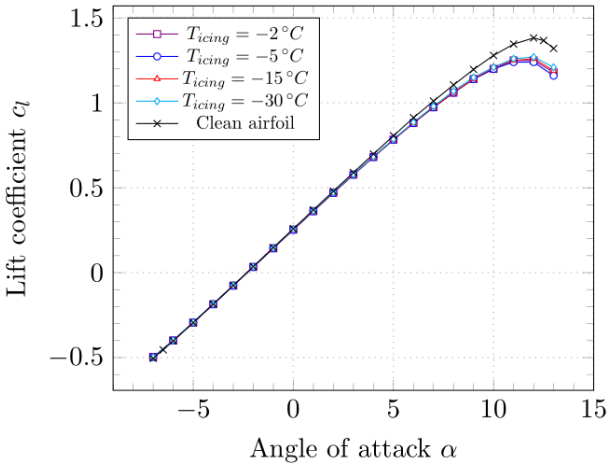

d) MVD 40 µm

Figure 9: Lift of the iced airfoils for MVDs a) 15 µm, b) 20 µm, c) 30 µm and d) 40 µm – Re = 800 000.

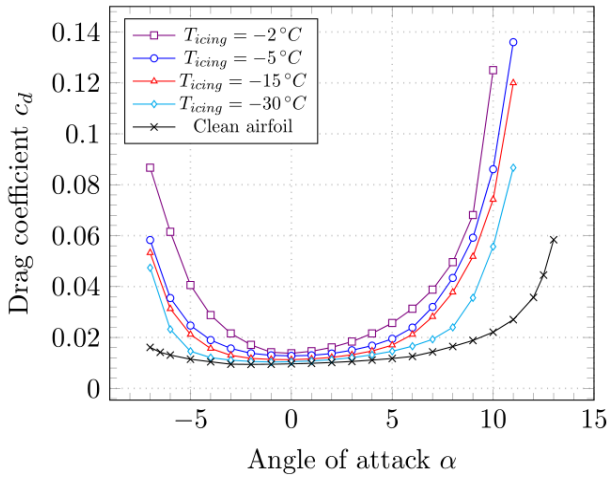

a) MVD 15 µm

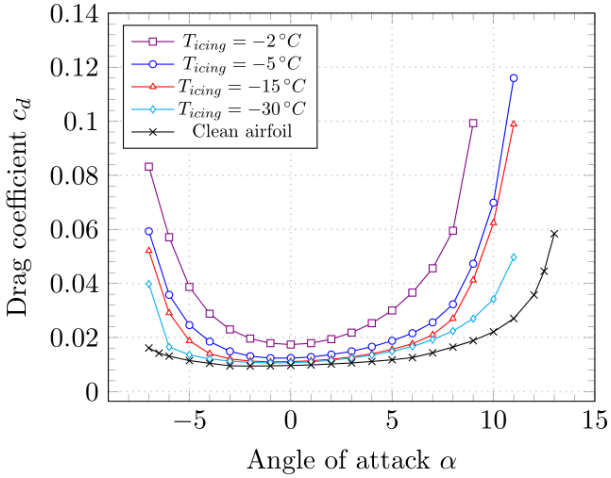

b) MVD 20µm

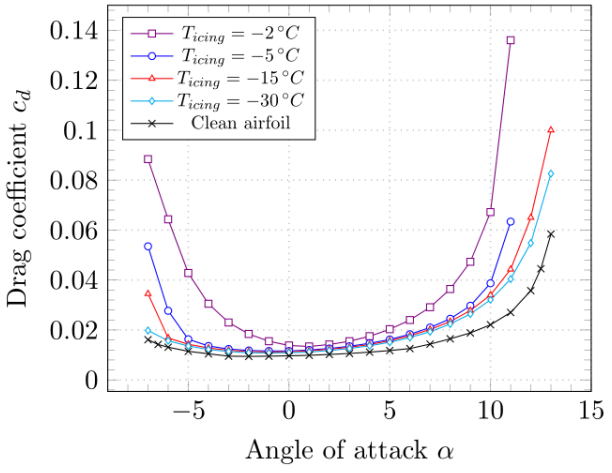

c) MVD 30µm

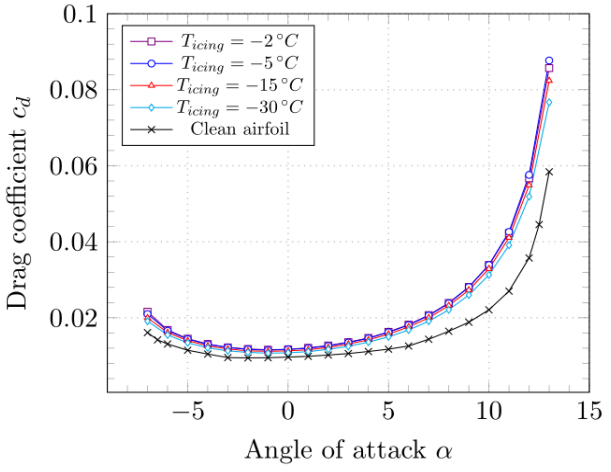

d) MVD 40µm

Figure 10: Drag of the iced airfoils for MVDs a) 15 µm, b) 20 µm, c) 30 µm and d) 40 µm – Re = 800 000.

DOI: 10.13009/EUCASS2019-240

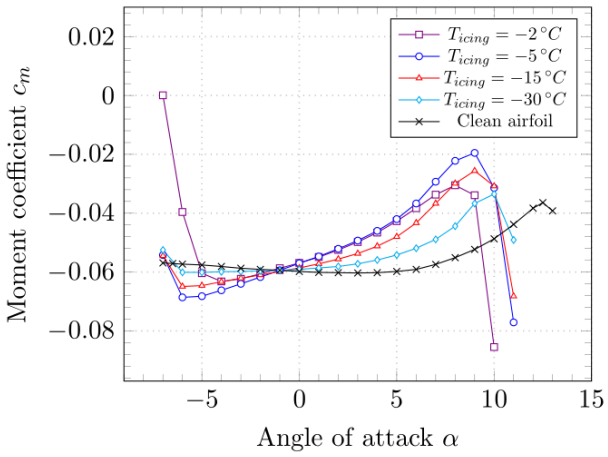

a) MVD 15 µm

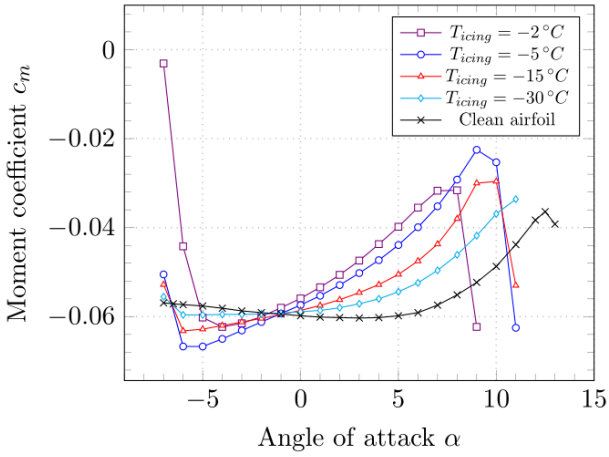

b) MVD 20 µm

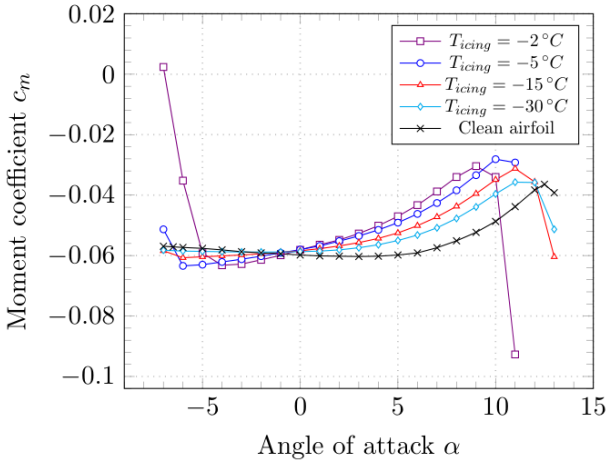

c) MVD 30 µm

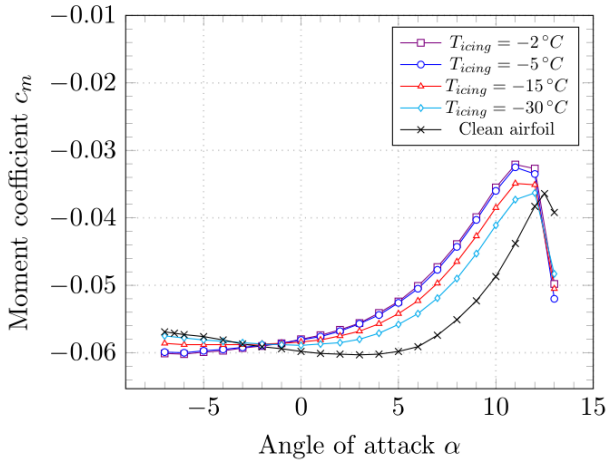

d) MVD 40 µm

Figure 11: Moment of the iced airfoils for MVDs a) 15 µm, b) 20 µm, c) 30 µm and d) 40 µm – Re = 800 000.

To visualize the different influences on the aerodynamic performance for all icing cases, an index for the lift, drag, stall AoA and the moment shall be introduced at this point. Three discrete points are representing the iced airfoil performance for lift and drag in comparison to the clean airfoil:

- **AoA 0°:** Smallest changes in drag compared to the clean airfoil and minor changes in lift
- **AoA 6°:** Limit of the quasi-static range of moment
- **Stall angle:** Maximum spread between iced and clean airfoil

For the moment index, two different discrete points are chosen:

- **AoA 0°:** Small changes in moment compared to the clean airfoil
- **AoA 4°:** Limit of the linear AoA range of the clean airfoil – maximum spread to the clean airfoil

The index is calculated with the following equation:

$$I_{lift} = \frac{1}{3}\left[\frac{\Delta\, C_{l\_stall}}{\Delta\, C_{l\_stall\_max}} + \frac{\Delta\, C_{l\_AoA6}}{\Delta\, C_{l\_AoA6\_max}} + \frac{\Delta\, C_{l\_AoA0}}{\Delta\, C_{l\_AoA0\_max}}\right] \quad (1)$$

All max-values (denominators) represent the difference between the clean airfoil value and the worst-case performance within all icing cases for the certain AoA. The numerator values are the difference between the clean airfoil performance and the respective value of the current icing case. As a result, the fractions and the overall index

DOI: 10.13009/EUCASS2019-240

can result in values $0 \leq I_{\text{lift}} \leq 1$. An index value of 1 represents the maximum deterioration of lift whereas a value of 0 would indicate no difference to the clean airfoil performance.

The drag, stall AoA and moment index values are calculated the same way, as described for the lift. The only difference for the stall AoA index is that the calculation consists of one instead of three fractions that describes the ratio between current stall angle reduction and worst-case stall angle reduction.

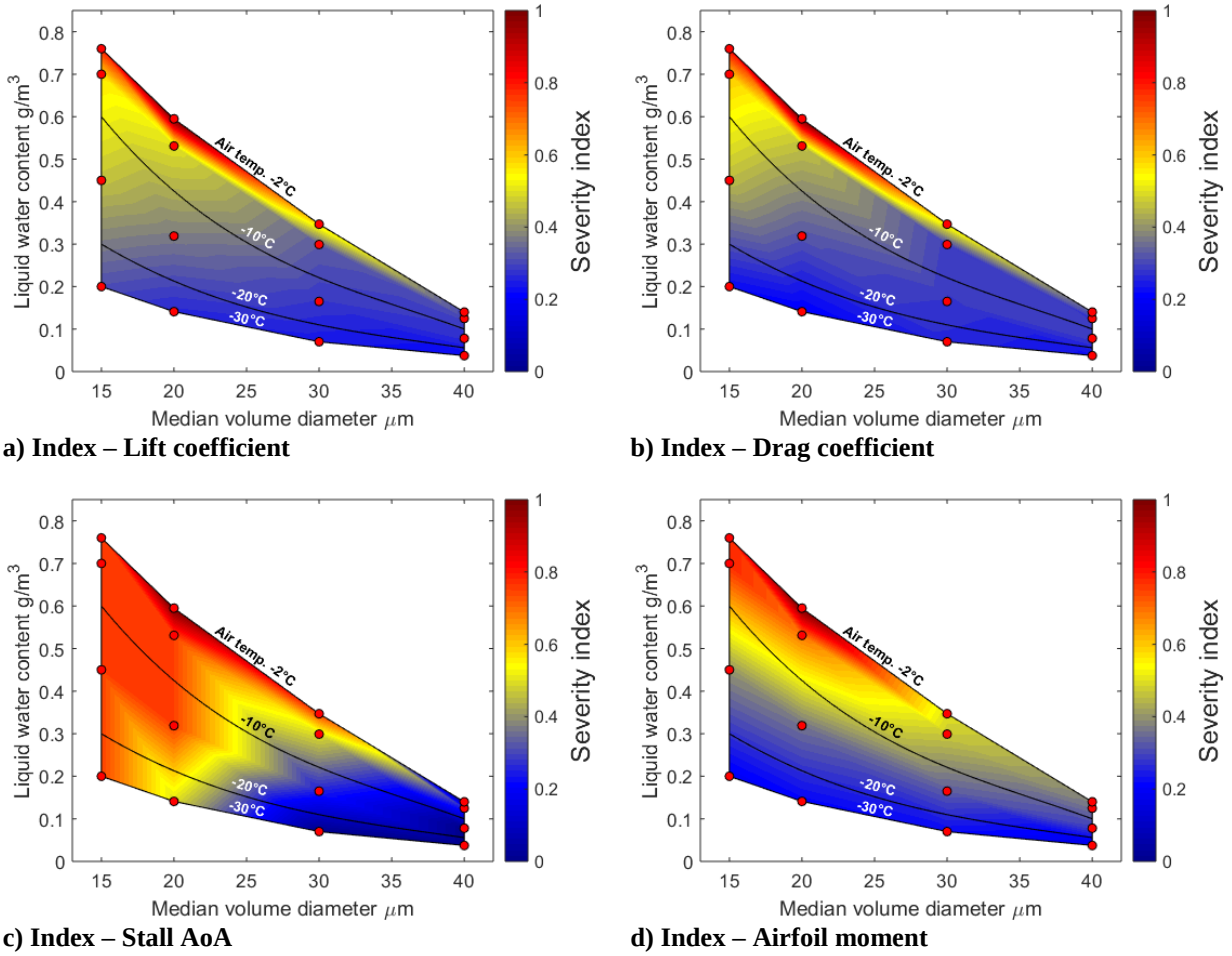

a) Index – Lift coefficient

b) Index – Drag coefficient

c) Index – Stall AoA

d) Index – Airfoil moment

Figure 12: a) Lift, b) drag, c) Stall AoA and d) moment change - Index visualization.

Figure 12 shows the index for each icing case as a color value. The areas between the discrete points that were investigated by simulation are determined by linear interpolation. The results for the lift and drag coefficient clearly show that the worst performance degradations can be found at temperatures close to 0 °C and high liquid water contents. Further, the influence of liquid water content at different droplet sizes can be noticed. At small droplet MVDs the LWC has a larger impact on the performance degradation. At larger droplet sizes, different LWCs show less impact on the performance. This can be explained with the decreasing LWC for bigger droplet MVDs. For example, at -30 °C/MVD 15 the LWC only differs slightly to the one at -2 °C/MVD 40. Also, the performance loss at both these points is almost similar. This behavior arises the impression that the droplet size has almost no impact on the performance degradation at low LWCs. For high temperatures however, different droplet sizes show a more significant influence.

The index visualization for the moment shows a distribution closely related to the one for lift and drag. The most severe icing conditions that result in highest lift reduction and highest drag increase also show the largest increase of the moment.

Besides changes in lift and drag and moment, Fig. 12 c) visualizes the change of maximum lift angles. Small droplet MVDs in combination with high LWCs lead to the smallest maximum lift angles, whereas large MVDs and low LWCs show no to minimal influence on the stall AoA. This gives a good insight on the general influence of different weather conditions on the maximum lift angle.

DOI: 10.13009/EUCASS2019-240

6. Discussion

Regarding the influence of the different weather parameters, larger LWC values have generally shown greater impact on the lift, drag and moment, whereas for droplet sizes, the greatest impact on performance have been identified at an MVD of 20 µm. However, the influence of only droplet size could not be determined, since the comparison of different droplet sizes at identical icing temperatures always includes different amounts of LWC (for the icing conditions identified by CFR 14, Part 25, App. C). For the investigation of droplet size influence only, further simulations, with constant LWC and constant icing temperature at different MVDs would be necessary.

In terms of maximum lift angle, the results clearly show that glaze ice horns have greater effect on the stall angle compared to more streamline shaped rime ice cases. However, the setup of simulations with 1° AoA steps and a maximum stall angle of 12° for the clean airfoil, restricts the resolution of stall angle degradation to a minimum of 8.5 %. and therefore, limits the validity of the results. Additional simulations with smaller AoA steps, would increase accuracy of the maximum lift angle prediction and give more detailed information on the influence of the different icing conditions on the stall angle. Depending on the flight envelope of the aircraft, further investigation, including the stall at negative AoAs could be of interest.

The results on the moment have revealed that all icing cases reduce the nose down moment of the airfoil. Since the overall aircraft's moment gradient must be $dc_m/d\alpha < 0$ for longitudinal static stability, all icing cases reduce this stability at first sight. However, further aircraft parameters such as the general aircraft configuration and icing of the horizontal stabilizer or even the elevator must be considered, to identify possible dangers on the aircraft's overall longitudinal stability. Therefore, apart from a reduced airfoil nose down moment compared to the clean airfoil, no statement about absolute aircraft stability can be made.

In terms of numerical methods, the validation of the iced airfoil performance in Fig. 5 showed that for severe ice shapes, the simulation setup with the SA model predicts an earlier onset of stall and therefore a higher performance degradation, compared to the experimental results. Different numerical methods, e.g. higher-level turbulence models might be more suitable in such cases. Additionally, the assumption that the airflow around iced airfoils is fully turbulent has not been verified and could be false. A partial laminar flow around iced airfoils, would not only affect the aerodynamic performance. As mentioned by Hann in [23], turbulent flow may also increase the evaporation rate and leads to earlier disappearance of water layers compared to laminar conditions. This points out the importance to investigate flow transition at iced airfoils further, not only to gain better understanding about the impact on aerodynamic performance, but also to successfully define energy requirements for an icing protection system. Therefore, more wind tunnel tests would be required, to validate the simulation results of the iced airfoils at the specific Reynolds number and to investigate flow transition on iced airfoils.

Also, the monodisperse distribution of droplet sizes for the ice accretion simulations is not likely to be found in reality. The Advisory Circular No 20-73A from the FAA suggests using a Langmuir-D distribution for droplet sizes up to 50 µm, for the icing certification of manned aircraft [20]. Since FENSAP-ICE already provides the Langmuir-D distribution within DROP3D, further simulations, using the FAA's suggested distribution, could give insight on the effect of differently distributed droplet sizes.

Overall, investigating the influence of different meteorological conditions on the aerodynamic performance including the identification of a worst-case condition at -2 °C/MVD 20 provides essential information for the development of an efficient IPS. The prevailing meteorological conditions that lead to the greatest performance degradation can be used for further simulations and wind tunnel tests to determine the maximum required heat flux of the icing protection system. The knowledge about the influence of different icing conditions on the aerodynamic performance can be used for the adaptation of flight controllers and control systems of IPSs. Based on the results for lift, drag, moment and AoA, flight controllers could adapt the flight envelope according to the present icing conditions to maximize the aircraft's aerodynamic efficiency.

In terms of adapting IPS control systems, the results provide useful information to maximize energy efficiency for example of a promising concept for an electro-thermal icing protection system with fully autonomous icing detection for UAVs, presented in [21] and [22]. The icing detection system operates intermittently to detect possible ice accretion. With the additional information on the influence of different icing conditions, the ice detection frequency could be reduced in less critical conditions to save electrical energy.

Finally, the identification of the worst-case icing condition is an essential finding, as earlier studies showed that the ambient temperature is a major factor for the power requirements of evaporative or running wet anti-icing systems [23]. With the worst-case icing condition at -2 °C/MVD 20 this study offers new information on the problem of how to operate an IPS.

DOI: 10.13009/EUCASS2019-240

7. Summary

In this study 16 different meteorological icing conditions have been investigated, using FENSAP-ICE simulation tool. Two different simulation models for the accretion of ice and the evaluation of aerodynamic performance have been set up. The ice accretion model has been validated with experimental data on a RG-15 airfoil from an icing wind tunnel. The ice accretion model has shown good capability of capturing the shape and extend of ice, depending on the prevailing weather conditions. The results show that the greatest ice masses occur at an MVD of 20 µm, compared by temperature.

Clean airfoil performance has been validated with literature data on the RG-15. Iced airfoil performance has been validated with literature data on an iced NREL S826 airfoil. The performance simulations have shown that all icing conditions affect the aerodynamic performance negatively. Generally, high liquid water contents and temperatures close to 0 °C show the greatest influence on the performance. Additionally, within all 16 different icing conditions, the worst-case condition for lift, drag and stall angle has been identified at an icing temperature of -2 °C and a droplet MVD of 20 µm.

In summary, the results are well suitable for comparison with each other, give a good insight on the influence of different meteorological conditions on the aerodynamic performance and provide essential new information for the development of an IPS for UAVs.

Author Contributions

Nicolas Fajt: acquisition of simulation data, analysis and interpretation of data, writing and editing of the manuscript
Richard Hann: provision of experimental data, study conception and design, analysis and interpretation of data, critical revision, supervision
Thorsten Lutz: provision of experimental data, supervision

Acknowlegdments

The research was funded by the Norwegian Research Council (project no. 223254) through the NTNU Centre of Autonomous Marine Operations and Systems (NTNU AMOS) at the Norwegian University of Science and Technology, and partially by CIRFA grant number 237906.

The author likes to thank Pointwise Inc. for providing a license, which enabled the generation of all grids using the latest version of the commercial mesh generation tool Pointwise. The author also likes to thank the ANSYS FENSAP-ICE support team, especially Jian Chen, who provided essential information for a successful setup of the simulations. Lastly, the author likes to thank the European Union for financial support of this work which was done as part of a master's thesis via an Erasmus program.

References

[1] Siquig, R. A., "Impact of Icing on Unmanned Aerial Vehicle (UAV) Operations," Technical Report, Naval Environmental Prediction Research Facility, 1990.
[2] Bragg, M. B., Broeren, A.P., and Blumenthal, L.A., "Iced-airfoil aerodynamics," Progress in Aerospace Sciences, vol. 41, 2005, pp. 323-362.
[3] Lindamae, P., Reyerson, C. C., and Kmiec, R., "Army Aircraft Icing," Technical Report ERDC/CRREL TR-02-13, US Army Corps of Engineers, September 2002.
[4] Szilder, K., and McIlwain, S., "In-Flight Icing of UAVs – The Influence of Reynolds Number on the Ice Accretion Process," SAE Technical Paper 2011-01-2572, October 2011.
[5] Koenig, G. G., Reyerson, C.C., and Kmiec, R., "UAV Icing Flight Simulation," 40th AIAA Aerospace Sciences Meeting & Exhibit, Reno, Nevada, 2002.
[6] Tran, P., Baruzzi, G., Tremblay, F., Benquet, P., Habashi, W. G., Petersen, P. B., Liggett, M. W., and Fiorucci, S., "FENSAP-ICE applications to unmanned aerial vehicles (UAV)," 42nd AIAA Aerospace Sciences Meeting and Exhibit, 2004, pp. 390-402.
[7] Hann, R., "UAV Icing: Comparison of LEWICE and FENSAP-ICE for Ice Accretion and Performance Degradation," 2018 Atmospheric and Space Environments Conference, Atlanta, Georgia, 2018.
[8] Habashi, W. G., Morency, F., and Beaugendre, H., "FENSAP-ICE: A Second Generation 3D CFD-based In-Flight Icing Simulation System," SAE Technical Paper 2003-01-2157, 2003.

DOI: 10.13009/EUCASS2019-240

[9] Bourgault, Y., Boutanios, Z., and Habashi, W. G., "Three-Dimensional Eulerian Approach to Droplet Impingement Simulation Using FENSAP-ICE, Part 1: Model, Algorithm, and Validation," Journal of Aircraft Vol. 37, No. 1, pp. 776-790, DOI 10.2514/2.2566, January-February 2000.
[10] Beaugendre, H., Morency, F., and Habashi, W. G., "FENSAP-ICE's Three-Dimensional In-Flight Ice Accretion Module: ICE3D," Journal of Aircraft Vol. 40, No.2, pp. 239-247, DOI 10.2514/2.3113, March-April 2003.
[11] Hann, R., Krøgenes, J., Brandrud, L., Bartl, J., Bracchi, T., and Sætran, L., "Experimental and Numerical Investigation of Icing Penalties of a UAV and Wind Turbine Airfoil at Low Reynolds Numbers," unpublished manuscript, 2019.
[12] Drela, M., "XFOIL: An Analysis and Design System for Low Reynolds Number Airfoils," MIT Dept. of Aeronautics and Astronautics, Cambridge, Massachusetts, 1989.
[13] Brandrud, L., and Krøgenes, L., "Aerodynamic Performance of the NREL S826 Airfoil in Icing Conditions," Master's thesis, NTNU, 2017.
[14] Hann, R., "UAV Icing: Ice Accretion Experiments and Validation," SAE Technical Paper 2019-01-2037.
[15] Federal Aviation Administration (FAA), "Part I – Atmospheric Icing Conditions," Title 14 CFR Part 25 Appendix C, Doc. No. 4080, 29 FR 17955, Amdt. 25-140, 79 FR 65528, Nov.4, 2014.
[16] Sartorius, D., "Hitzdrahtmessungen zur Grenzschicht- und Nachlaufentwicklung bei Ablöseblasen in der Nähe der Profilhinterkante," Diplomarbeit, Stuttgart, July 2001.
[17] Selig, M. S., Guglielmo, J. J., Broeren, A. P., and Giguère, P., "Summary of Low-Speed Airfoil Data," Vol. 1, SoarTech Publications, 1995.
[18] Szilder, K., and Yuan, W., "The Influence of Ice Accretion on the Aerodynamic Performance of a UAS Airfoil," 53rd AIAA Aerospace Science Meeting, 2015, p. 536.
[19] SAE International Group, "Icing Wind Tunnel Interfacility Comparison Tests," Aerospace Information Report AIR5666, SAE Aerospace, 2012.
[20] Federal Aviation Adminstration (FAA), "Aircraft Icing Protection," Advisory Circular No 20-73A, 2006.
[21] Sørensen, K., and Johansen, T. A., "Flight Test Results for Autonomous Icing Protection Solution for Small Unmanned Aircraft," 2017 International Conference on Unmanned Aircraft Systems ICUAS, 2017, pp. 971-980.
[22] Hann, R., Borup, K, Zolich, A., Sørensen, K., Vestad, H., Steinert, M., and Johansen, T. A., "Experimental Investigations of an Icing Protection System for UAVs," SAE Technical Paper 2019-01-2038, 2019.
[23] Hann, R., "UAV Icing: Comparison of LEWICE and FENSAP-ICE for Anti-Icing Loads," AIAA SciTech Forum, 2019.